Preclinical validation of anti-TMEFF2-auristatin E–conjugated antibodies in the treatment of prostate cancer

Daniel E.H. Afar,[1] Vinay Bhaskar,[1] Eric Ibsen,[1] Danna Breinberg,[1] Susan M. Henshall,[2] James G. Kench,[2,5] Marija Drobnjak,[6] Rick Powers,[1] Melanie Wong,[1] Ferdinand Evangelista,[1] Chris O'Hara,[1] David Powers,[1] Robert B. DuBridge,[1] Ingrid Caras,[1] Ruth Winter,[7] Terri Anderson,[1] Nanette Solvason,[7] Phillip D. Stricker,[3] Carlos Cordon-Cardo,[6] Howard I. Scher,[6] John J. Grygiel,[4] Robert L. Sutherland,[2] Richard Murray,[1] Vanitha Ramakrishnan,[1] and Debbie A. Law[1]

[1]Protein Design Labs, Inc., Fremont, California; [2]Garvan Institute of Medical Research and Departments of [3]Urology and [4]Medical Oncology, St. Vincent's Hospital, Darlinghurst, Sydney, New South Wales, Australia; [5]Department of Tissue Pathology, Institute of Clinical Pathology and Medical Research, Westmead Hospital, Westmead, New South Wales, Australia; [6]Memorial Sloan Kettering Cancer Center, New York, New York; and [7]Eos Biotechnology, Inc., Fremont, California

Abstract

Current treatments for advanced stage, hormone-resistant prostate cancer are largely ineffective, leading to high patient mortality and morbidity. To fulfill this unmet medical need, we used global gene expression profiling to identify new potential antibody-drug conjugate (ADC) targets that showed maximal prostate cancer-specific expression. *TMEFF2*, a gene encoding a plasma membrane protein with two follistatin-like domains and one epidermal growth factor–like domain, had limited normal tissue distribution and was highly overexpressed in prostate cancer. Immunohistochemistry analysis using a specific monoclonal antibody (mAb) to human TMEFF2 showed significant protein expression in 74% of primary prostate cancers and 42% of metastatic lesions from lymph nodes and bone that represented both hormone-naïve and hormone-resistant disease. To evaluate anti-TMEFF2 mAbs as potential ADCs, one mAb was conjugated to the cytotoxic agent auristatin E via a cathepsin B–sensitive valine-citrulline linker. This ADC, Pr1-vcMMAE, was used to treat male severe combined immunodeficient mice bearing xenografted LNCaP and CWR22 prostate cancers expressing TMEFF2. Doses of 3 to 10 mg/kg of this specific ADC resulted in significant and sustained tumor growth inhibition, whereas an isotype control ADC had no significant effect. Similar efficacy and specificity was shown with huPr1-vcMMAE, a humanized anti-TMEFF2 ADC. No overt *in vivo* toxicity was observed with either murine or human ADC, despite significant cross-reactivity of anti-TMEFF2 mAb with the murine TMEFF2 protein, implying minimal toxicity to other body tissues. These data support the further evaluation and clinical testing of huPr1-vcMMAE as a novel therapeutic for the treatment of metastatic and hormone-resistant prostate cancer. [Mol Cancer Ther 2004;3(8):921–32]

Introduction

Prostate cancer kills 30,000 men every year in the United States and is the second leading cause of cancer death among American males (see http://www.cancer.org/docroot/STT/stt_0.asp). Locally confined disease is often successfully treated with surgery (radical prostatectomy) and/or radiotherapy. However, nearly 30% of patients relapse with distant metastases to bone and other organs. Hormone ablation therapy is the primary therapeutic option for advanced disease but ultimately leads to the incurable hormone-resistant form of prostate cancer (1). Although some taxol-based therapies are in experimental phase of development for hormone-independent disease (2–4), prostate cancer is relatively resistant to current chemotherapies (5).

One of the many approaches under evaluation for the treatment of cancers in experimental systems and the clinic is the use of antibody-drug conjugates (ADC; refs. 6–14). The strategy of this approach is to target a cancer-specific antigen with a highly specific antibody that can deliver a toxic payload to the cancer cell. This specific targeting of cancer cells allows for the toxic payload to possess much greater potency than conventional cancer chemotherapeutics while reducing the risk of toxic side effects (11). Ideally, and by one strategy (9), the potent drug is internalized via the antibody-antigen complex released within the cell and specifically kills the cancer cells. To minimize toxic side effects, it is critical that the molecular target is not expressed in essential organs that are accessible to circulating antibodies. In addition, the target must be at the plasma membrane of cancer cells to allow antibody access and preferably should not be shed into the serum, which might create a potential sink for the therapeutic ADC.

Received 4/9/04; revised 5/24/04; accepted 6/15/04.

Grant support: National Health and Medical Research Council of Australia, Prostate Cancer Foundation of Australia, R.T. Hall Trust, and Cancer Council New South Wales (R.L. Sutherland); Prostate Cancer Foundation and PepsiCo (H.I. Scher and C. Cordon-Cardo).

The costs of publication of this article were defrayed in part by the payment of page charges. This article must therefore be hereby marked advertisement in accordance with 18 U.S.C. Section 1734 solely to indicate this fact.

Note: D.E.H. Afar and V. Bhaskar contributed equally to this work. R. Winter is currently at Raven Biotechnologies, Inc., South San Francisco, CA 94080. N. Solvason is currently at Bayhill Therapeutics, Inc., Palo Alto, CA 94303.

Requests for reprints: Daniel E.H. Afar, Protein Design Labs, Inc., 34801 Campus Drive, Fremont, CA 94555. Phone: 510-574-1665; Fax: 510-574-1661. E-mail: dafar@pdl.com

Recent advances in gene expression profiling have led to the identification of numerous cancer-specific antigens, some of which may show suitable selectivity to function as an ADC target in prostate cancer (8, 15–19). We combined gene expression profiling of prostate cancer and normal human body tissues with bioinformatics analysis to select the best possible ADC targets for prostate cancer. One of these genes encodes the TMEFF2 protein (20), also known as tomoregulin (21), TPEF (22), and TENB2 (23). Little is known about the biological function of TMEFF2, although an experimentally generated soluble form of TMEFF2 extracellular domain activates HER4 kinase activity in MKN28 gastric cancer cells (21) and promotes the survival of central nervous system neurons in culture (20).

Here, we report that TMEFF2 is highly expressed in prostate cancer at all stages of the disease including metastastic and hormone-independent disease. We also show that TMEFF2 is a strong candidate for an ADC-based therapeutic approach, particularly due to its rapid internalization into cancer cells when ligated with an antibody and/or an ADC. When auristatin E, a drug related to the dolastatin 10 family of microtubule inhibitors (8–10), was conjugated to anti-TMEFF2-specific antibodies, this ADC specifically killed TMEFF2-expressing cancer cells *in vitro* and significantly inhibited prostate cancer xenograft growth *in vivo*, with no signs of overt toxicity to the mice. Specifically, auristatin E was conjugated to anti-TMEFF2 antibodies via a cathepsin B–sensitive linker, creating an ADC with an average of seven to eight drug molecules per antibody. Internalization of the ADC into cathepsin B–rich vesicles results in liberating the drug inside the cells as described (8–10). The selected anti-TMEFF2 monoclonal antibody (mAb) recognizes both murine and human proteins with similar affinities, making the lack of detectable toxicity in mice treated with the ADC more significant. Our preclinical results validate anti-TMEFF2 ADC as a potential therapeutic for the treatment of metastatic and hormone-resistant prostate cancer.

Materials and Methods

DNA Microarray Analysis

Primary tumor tissue from 74 prostate cancer patients and 347 samples of nonmalignant adult tissues were collected and processed for gene expression profiling using Hu03, a customized Affymetrix GeneChip (Santa Clara, CA), as published previously (8, 19, 24). The clinical parameters of the radical prostatectomy cohort, gene array data on the prostate cancer cohort, data mining methods for cancer antigens, and bioinformatics analysis were described previously in detail (8, 19, 24).

To identify prostate cancer genes, gene expression ratios of prostate cancer to normal body tissues were calculated for all 59,619 probesets on the Hu03. After sorting all probesets by ratio, genes with the highest prostate cancer to normal adult tissue expression ratios were selected for further evaluation if their encoded sequences contained predicted transmembrane domains and/or other structural domains that suggested localization of the gene product to the plasma membrane.

Cloning of *TMEFF2* and Generation of TMEFF2-Fc Fusion

Total RNA was isolated from LNCaP cells using TRIzol reagent (Invitrogen, Carlsbad, CA). cDNA was produced from total RNA (1 μg) using SuperScript II (Invitrogen). The *TMEFF2* cDNA was cloned from LNCaP cDNA (50 ng) using PCR containing Advantage II polymerase (BD Biosciences Clontech, Palo Alto, CA) and the two outside primers *TMEFF2* RT 5′-TTGCTGCTGCAGAGTTGCACGAAC and *TMEFF2* RT 3′-AGTCCAGCCACTGTGAAACATGCTC followed by nested PCR using the cloning primers *TMEFF2* 5′-AGGTTAATTAACATGGTGCTGTGGGAGTCCCC and *TMEFF2*-Fc 3′-TAAGCGGCCGCTCGTACAGGACCGGGAACAACG. The products of this reaction were cloned into *Pac*I (5′)/*NotI* (3′) sites of a modified pBMN-Z-I-Blast vector (G. Nolan, Stanford University, Stanford, CA), resulting in an in-frame fusion between the extracellular domain of the *TMEFF2* gene and the constant region of the human IgG γ1 heavy chain gene.

Murine *TMEFF2* was cloned by PCR using clone 1397175 from the Integrated Molecular Analysis of Genomes and Their Expression Consortium as template and the two outside primers Mu *TMEFF2* RT 5′-TTCTTCAGAAGCCTTTGGTTGCTGC and Mu *TMEFF2* RT 3′-TAGTCCAAGCTGTTGGTTGTCCGG followed by nested PCR using the cloning primers Mu *TMEFF2* Cloning 5′-AGGTTAATTAACATGGTGCTGTGGGAGTCCCC and Mu *TMEFF2*-Fc 3′-TATGCGGCCGCGCCAGGAACAACGTAGAGAACAC. Rat *TMEFF2* was cloned by PCR using total rat brain RNA (BD Biosciences Clontech) as template and the two outside primers rat *TMEFF2* 1F 5′-TTGCTGCTGCAGAGTTGCACGAAC and rat *TMEFF2* 1F 3′-AGTCCAGCCACTGTGAAACATGCTC followed by nested PCR using the cloning primers Mu *TMEFF2* Cloning 5′-AGGTTAATTAACATGGTGCTGTGGGAGTCCCC and Mu *TMEFF2*-Fc 3′-TATGCGGCCGCGCCAGGAACAACGTAGAGAACAC (sequence of murine and rat *TMEFF2* are identical in these regions). Rat and murine TMEFF2-Fc fusions were generated as described above for human TMEFF2.

Generation of Anti-TMEFF2 Antibodies

Female BALB/c mice (Taconic Farms, Germantown, PA) were immunized with TMEFF2-Fc fusion protein. mAbs were generated by standard techniques with spleen cells being fused to the P3X_63_Ag8.653 fusion partner (American Type Culture Collection, Manassas, VA). A panel of TMEFF2-specific antibodies were identified using a variety of techniques including ELISA on TMEFF2 protein, Western blotting, and fluorescence-activated cell sorting analysis on TMEFF2-expressing cell lines.

Kinetic Analysis of Anti-TMEFF2 Antibodies by Surface Plasmon Resonance

Kinetics measurements between human TMEFF2-Fc fusion protein and TMEFF2 mAb Pr1#19 were done using BIAcore 3000 (BIAcore, Piscataway, NJ). Pr1#19 was

immobilized with 100 resonance units on a research-grade CM5 sensor chip by the BIAcore amine coupling reagents [*N*-ethyl-*N*′-dimethylaminopropylcarbodiimide, *N*-hydroxysuccinimide, and ethanolamine HCl (pH 8.5)]. Assays were run at a flow rate of 30 μL/min at room temperature. A three-minute association phase of each TMEFF2-Fc was followed by 10-minute injection of running buffer [10 mmol/L HEPES, 300 mmol/L NaCl, 3 mmol/L EDTA, 0.05% P-20 (pH 7.4)] to monitor dissociation. The mAb surface was regenerated with NaOH (25 mmol/L). The binding kinetics of each TMEFF2-mAb pair was calculated from the data at six different concentrations (2,048, 512, 128, 32, 8, and 2 nmol/L) of TMEFF2-Fc analyte using the BIAevaluate program. Double referencing was applied in each analysis to eliminate background responses from reference surface and buffer-only control. The affinity (K_D) of binding was obtained by simultaneously fitting the association and dissociation phases of the sensorgram from the analyte concentration series using the bivalent analyte model from the BIAevaluate software.

Cross-reactivity of TMEFF2 from different species (mouse, rat, and human) with Pr1#19 was determined by comparing their affinities using each species' TMEFF2-Fc as analyte onto the Pr1#19 surface.

Cloning of Hybridoma Variable Domains and Generation of Chimeric and Humanized IgG1/κ Antibody

cDNAs encoding variable heavy and light domains of the Pr1#19 antibody were cloned from hybridoma cells. Total RNA was prepared using the RNeasy kit (Qiagen, Valencia, CA), and cDNA was prepared from total RNA using a SMART RACE kit (BD Biosciences Clontech). Variable heavy and light domains were PCR amplified from cDNA using 5′ RACE primers and 3′ primers complementary to murine IgG1 and κ constant domains, and the PCR fragments were cloned into the pCR4 Blunt TOPO vector (Invitrogen). The cloned variable heavy and light domains were reamplified by PCR using primers to append appropriate flanking restriction endonuclease sites for cloning into expression vectors containing human IgG1 and κ constant domains. The final expression vectors (DEF39.PDM9.19.H and NEF39.PDM9.19.κ) directed expression of chimeric IgG1 heavy and κ light chains using the Chinese hamster EF-1a promoter in Chinese hamster ovary cells (Icos Corporation, Seattle, WA).

The variable heavy and light domains of the Pr1#19 chimera were humanized by grafting the murine complementarity determining regions as defined by Kabat et al. (25) onto acceptor human framework regions. Molecular modeling was done to identify a few key murine framework residues to be retained in the final design to maintain complete murine complementarity determining region function in the context of the human frameworks (26). Sequence 21u-51 (27) was used for the heavy chain, and sequence EL-25 (28) was used for the light chain; both were selected because of high level of sequence similarity to the respective sequences of Pr1#19. Based on molecular modeling, murine framework residues expected to influence complementarity determining region conformation were retained at positions 1, 27, 30, 48, 67, and 71 of the heavy chain using the Kabat et al. numbering system (25); no murine framework residues were retained in the humanized light chain. In addition, residue 23 of the heavy chain and residues 10, 70, and 104 of the light chain were changed to more commonly occurring amino acid types in human sequences (26). The humanized variable domains were synthesized from overlapping 40-mer oligonucleotides (29), sequence verified, and cloned into the same expression vectors as were used for the chimera to generate expression plasmids DEF39.PDM9.19.VH3 and NEF39.PDM9.19.VL3.

Tissue Microarrays and Immunohistochemistry

Medium density tissue microarrays (Beecher Instruments, Silver Spring, MD) of primary prostate cancer tissue were generated with 1.0 mm tissue core biopsies as described by Kononen et al. (30). These included tissues from 65 patients with localized disease, 5 patients with pelvic lymph node metastases collected at radical prostatectomy, and 5 prostate cancer specimens from previously untreated patients with bony metastatic disease (defined as D2 specimens) who underwent transurethral resection of the prostate (arrays and slides generated at the Garvan Institute of Medical Research, Sydney, New South Wales, Australia). Tissue arrays incorporating advanced metastatic prostate cancer included specimens from hormone-sensitive and hormone-independent cancers sampled primarily from metastases to lymph node and bone (arrays generated at Memorial Sloan Kettering Cancer Center, New York, NY).

Normal body tissue specimens were collected from samples harvested at the time of cadaveric organ donation from six individuals (three males and three females obtained from Zoion, Hawthorne, NY). Additional normal tissue samples were derived from commercially available tissue microarrays (Clinomics BioSciences, Inc., Pittsfield, MA).

Immunohistochemistry (IHC) using Pr1#19 was done on formalin-fixed paraffin embedded tissues using standard methods described previously (19).

Cell Culture and Transfections

All tissue culture reagents were obtained from Invitrogen unless otherwise noted. LNCaP-FGC and PC3 were obtained from the American Type Culture Collection. LNCaP-FGC cells were maintained in phenol-red free Iscove's modified Dulbecco's medium containing 10% low IgG fetal bovine serum (Invitrogen-Life Technologies, Inc., Gaithersburg, MD), 2 mmol/L L-glutamine, 1 mmol/L sodium pyruvate, and 1× nonessential amino acids (Invitrogen-Life Technologies). PC3 cells were cultured as detailed by American Type Culture Collection. For the establishment of stable cell lines, monolayers of PC3 were transfected with retroviral vector pBMN-Z-I-Blast encoding full-length TMEFF2 with a COOH-terminal hemagglutinin tag using LipofectAMINE 2000 (Invitrogen). Cells were selected in medium containing blasticidin (5 μg/mL; Invitrogen-Life Technologies) and screened for TMEFF2 expression by flow cytometry.

Flow Cytometry

Cells were removed with EDTA (5 mmol/L) in Tris-HCl (pH 8.0) and blocked by centrifugation in HBSS containing 3% heat-inactivated fetal bovine serum, 1% normal goat serum (Sigma-Aldrich, St. Louis, MO), and 1% bovine serum albumin at 4°C for 5 minutes. Cells were incubated for 30 to 60 minutes at 4°C with anti-TMEFF2 (10 μg/mL) in fluorescence-activated cell sorting buffer (PBS containing 0.1% bovine serum albumin). After washing in fluorescence-activated cell sorting buffer, cells were resuspended in FITC anti-mouse IgG (heavy + light) antibody (1:50 dilution, Caltag Laboratories, Burlingame, CA) for 30 to 60 minutes at 4°C. Cells were washed and resuspended in fluorescence-activated cell sorting buffer containing propidium iodide (1 μg/mL). Fluorescence intensity was measured on a FACScan (BD Biosciences, San Jose, CA).

Immunofluorescence and Internalization Assay

PC3 and PC3-TMEFF2 cells grown on coverslips were incubated with medium containing Pr1#19 (10 μg/mL) at 4°C for 1 hour. Antibody binding was detected using AlexaFluor-488 goat anti-mouse secondary antibody (1:2,200 dilution, Invitrogen-Molecular Probes, Eugene, OR). Cells were washed and fixed using 5% ultrapure formaldehyde in PBS for 40 minutes. Slides were mounted using Permafluor (Beckman-Coulter, Miami, FL) for visualization. For internalization, cells were placed in an incubator at 37°C for 1 hour and placed on ice for 1 hour in blocking solution (20 μg/mL pure goat anti-mouse antibody in medium). After washing in PBS, cells were fixed in 5% ultrapure formaldehyde. Cells were washed with 0.5% Triton X-100 and incubated with AlexaFluor-594 goat anti-mouse secondary antibody (1:2,200 dilution, Invitrogen-Molecular Probes). Staining was visualized with a Nikon E800 fluorescence microscope (Nikon, Melville, NY).

ADC Chemistry

Purified anti-TMEFF2 mAb or control murine IgG1 TIB191 were conjugated to valine-citrulline-monomethyl auristatin E (maleimide-vcMMAE, Seattle Genetics, Bothell, WA) as described by Bhaskar et al. (8). Purified antibody (either murine Pr1#19, humanized Pr1#19, or control murine IgG1) were reduced with DTT (10 mmol/L). Thiol content was determined by measuring $A_{412\ nm}$ after incubation with Ellman's reagent and subsequent calculation. Equimolar maleimide-vcMMAE solution (8 mmol/L in DMSO) in cold acetonitrile (20% final concentration) was incubated with reduced mAb for 30 minutes at 4°C. Unconjugated vcMMAE was removed by dialysis at 4°C into PBS and filtered. Conjugated mAb was quantified using $A_{280\ nm}/A_{260\ nm}$, and the extent of aggregate versus monomer was determined by size exclusion high-performance liquid chromatography. Finally, matrix-assisted laser desorption/ionization time of flight was used to determine the number of drug molecules per mAb.

In vitro Growth Assays

Parental and TMEFF2-transfected PC3 cell lines were plated at a density of 2,500 cells/well in 96-well plates and allowed to recover overnight in phenol-free Iscove's modified Dulbecco's medium containing 10% fetal bovine serum and supplements (growth medium). Cell growth in the presence of ADC was determined as described by Bhaskar et al. (8). Cells were challenged for 1 hour with mAb or ADC in Iscove's modified Dulbecco's medium at the indicated concentrations. Cells were washed twice with growth medium and allowed to proliferate in fresh growth medium for 4 days. Cell viability was assessed using the CellTiter 96 AQueous Non-Radioactive Cell Proliferation Assay (Promega Biosciences, San Luis Obispo, CA). All growth studies were done at least three times in triplicate.

Animal Studies

Tumor treatment studies were done in 6- to 12-week-old (~20 g in weight) male immune compromised CB-17 severe combined immunodeficient mice (strain C.B-Igh1/IcrTac-Prkdc, Taconic Farms). LNCaP-FGC cells were inoculated at 1×10^7 cells in 50:50 volume of Iscove's modified Dulbecco's medium-Matrigel s.c. on the right flank of animals. CWR22 xenografts were generously provided by Dr. Tom Pretlow (Case Western Reserve University Medical Center, Cleveland, OH) and were s.c. implanted as tumor fragments. Tumors were allowed to establish until reaching an average of 50 to 100 mm^3 as determined by caliper measurement and calculated by $\pi/6 \times$ length $\times$ width $\times$ height. Animals were randomized into groups for each of the desired treatment arms. ADCs were delivered either i.p. or i.v. every 4 days (for 6–12 doses as indicated). Dosing was based on the calculation of drug equivalent (using auristatin E molecular weight of 708) of each ADC. The indicated concentration corresponding to the complete ADC (antibody + auristatin E + linker) was an approximation based on the number of auristatin E molecules conjugated (usually six to eight) per antibody for each ADC preparation. Tumor volume was measured twice weekly, and clinical and mortality observations were done daily according to Institutional Animal Care and Use Committee regulations.

Results

Expression of TMEFF2 in Prostate Cancer

In an effort to identify potential ADC targets in prostate cancer, gene expression profiles of 74 prostate cancers (8, 19, 24) were compared with 347 normal adult tissue samples representing 58 different organs. The goal was to identify genes that are up-regulated in prostate cancer and that encode proteins localized to the cell surface for antibody accessibility. These genes should also exhibit little to no expression in vital organs to minimize target-driven undesirable side effects of the ADC. Genes with the desired expression profile were triaged by extensive bioinformatics analysis to determine their structural and functional classification and their potential for cell surface localization.

The *TMEFF2* gene (National Center for Biotechnology Information reference sequence NM_016192.2; ref. 21) displayed all the desired characteristics. The median TMEFF2 mRNA expression level in prostate cancer [550 average

intensity units (AIU)] exhibited a 16-fold increase with respect to the 85th percentile of normal body tissue expression (34 AIU; Fig. 1A). Expression was also detected in the central nervous system (median expression of 267 AIU among 22 samples) and normal prostate (median expression of 397 AIU among 7 prostates) as described previously (20, 23). No expression was detected in 36 other normal tissues tested. Among nonprostate cancer tissues, lower levels of *TMEFF2* expression were also detected in low-grade glioblastoma but not in other carcinomas, including those of the colon, breast, ovary, lung, pancreas, and kidney (data not shown). Significant *TMEFF2* expression was also detected in two prostate cancer tumor lines LNCaP and CWR22 (Fig. 1B), which were originally derived from advanced stage prostate cancer (31, 32). The gene chip expression data were confirmed by Taqman analysis of the same samples (data not shown). Bioinformatics analysis of the *TMEFF2* gene sequence suggested that the protein product contains a signal sequence and a single transmembrane domain and is predicted to localize to the plasma membrane, making it a suitable candidate target for therapeutic antibodies.

Protein Expression of TMEFF2 in Normal and Malignant Tissues

To study TMEFF2 protein expression, mAbs were generated by immunizing mice with a Fc fusion protein of the extracellular domain of human TMEFF2. From an initial pool of ~100 hybridoma supernatants, 12 anti-TMEFF2

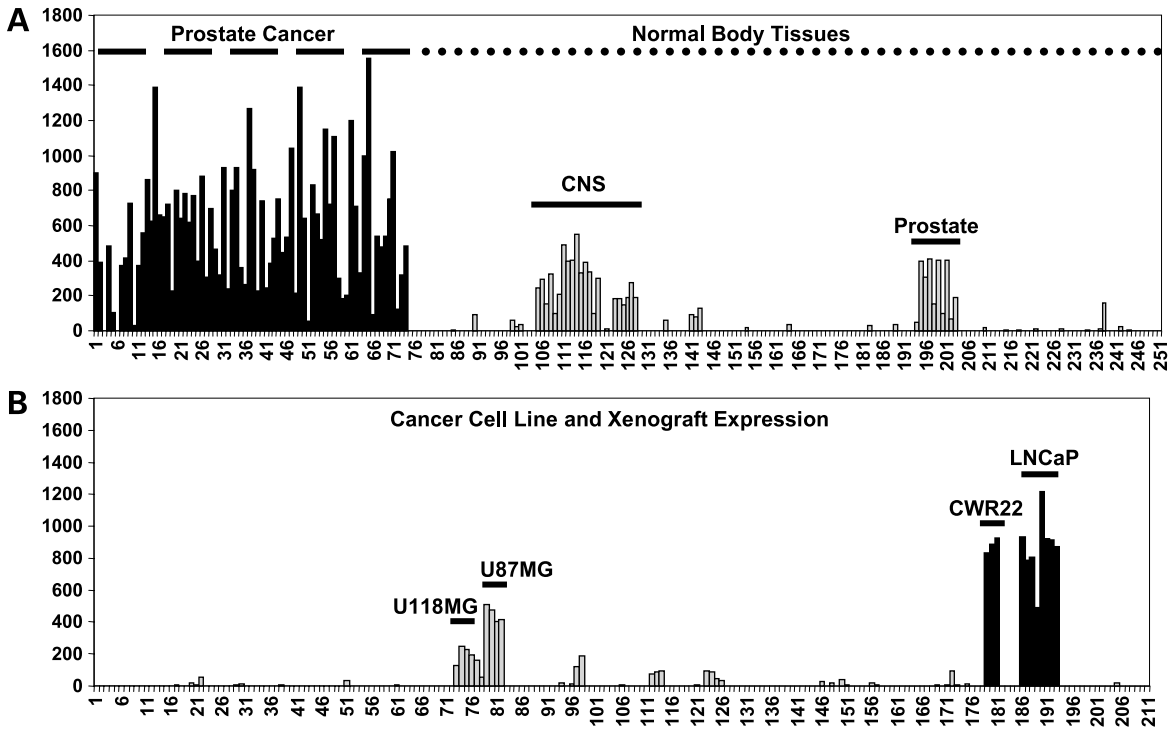

Figure 1. Gene expression of *TMEFF2* in prostate cancer. **A,** TMEFF2 mRNA detected by gene microarray analysis in prostate cancer samples and normal body tissues. *Y axis,* AIUs. *X axis,* samples: prostate cancer (*black*, *1–74*), adipose tissue (*75–77*), adrenal glands (*78–80*), aorta (*81–83*), appendix (*84–86*), artery (*87–89*), bladder (*90–92*), bone marrow (*93–95*), breast (*96–98*), colonic epithelium (*99–101*), cervix (*102–104*), brain (*105–107*), cerebral cortex (*108–110*), corpus callosum (*111–113*), dorsal root ganglia (*114–116*), hypothalamus (*117–119*), pituitary (*120–122*), spinal cord (*123–125*), thalamus (*126–128*), colon (*129–131*), diaphragm (*132–134*), epididymis (*135–137*), esophagus (*138–140*), gallbladder (*141–143*), heart (*144–146*), kidney (*147–149*), liver (*150–152*), lung (*153–155*), lymph node (*156–158*), muscle (*159–161*), ovary (*162–164*), stomach (*165–167*), vagus nerve (*168–170*), omentum (*171–173*), larynx (*174–176*), lip (*177–179*), oral mucosa (*180–182*), pharyngeal mucosa (*183–185*), tongue (*186–188*), pancreas (*189–191*), peripheral blood mononucleocytes (*192–194*), prostate (*196–201*), retina (*202–203*), salivary gland (*204–206*), skin (*207–209*), small intestine (*210–212*), spleen (*213–215*), stomach (*216–218*), synovium (*219–221*), testis (*222–224*), thymus (*225–227*), thyroid and parathyroid glands (*228–230*), tonsils (*231–233*), trachea (*234–236*), ureter (*237–239*), urethra (*240–242*), uterus (*243–245*), vagina (*246–248*), and saphenous vein (*249–251*). **B,** *TMEFF2* mRNA detected by gene microarray analysis in cancer cell lines and xenografts. *Y axis,* AIUs. *X axis,* samples listed by cancer of origin. Bladder cancer lines: HT1376 (*1–4*), SW780 (*5–8*), and UMUC3 (*9–12*); breast cancer lines: BT474 (*13–16*), MB231 (*17–20*), MB435s (*21–23*), MB453 (*24–27*), MCF7 (*28–31*), and NW231 (*32–35*); B-cell lymphoma lines: CA46 (*36*), EB1 (*37*), PZ-HPV7 (*38*), RAJI (*39*), and RAMOS (*40*); colon cancer lines: EB (*41–44*), HCT116 (*45–48*), HT29 (*49–52*), SW480 (*53–56*), and SW620 (*57–60*); cervical cancer lines: HT3 (*61–64*), ME180 (*65–68*), and SiHa (*69–72*); Ewing sarcoma lines: RDES (*73*) and SKES (*74*); glioblastoma lines: U118MG (*75–78*) and U87MG (*79–83*); head and neck cancer lines: A253 (*84–87*) and FaDu (*88–91*); lung cancer lines: A549 (*92–95*), H23 (*96–99*), H358 (*100–103*), CALU6 (*104–107*), H460 (*108–111*), H345 (*112–114*), H69 (*115–119*), H157 (*120–122*), and H520 (*123–126*); melanoma lines: A375 (*127–131*), C32 (*132–135*), C8161 (*136–139*), and SKMEL28 (*140–143*); ovarian cancer lines: CSOC-882.2 (*144–147*), ES-2 (*148–151*), OV90 (*152–155*), OVCAR3 (*156–159*), PA-1 (*160–162*), and SKOV3 (*163–166*); pancreatic cancer lines: BxPC3 (*167–170*), Panc1 (*171–174*), and MiaPaCa2 (*175–178*); prostate cancer lines (*black*): CWR22 (*179–181*), DU145 (*182–185*), LNCaP (*186–193*), PC3 (*194–197*), and RPWE-2 (*198–200*); renal cancer lines: TR-786-0 (*201–204*) and TR-SN12-C (*205–207*); and T-cell lymphoma line: Karpas (*208–211*).

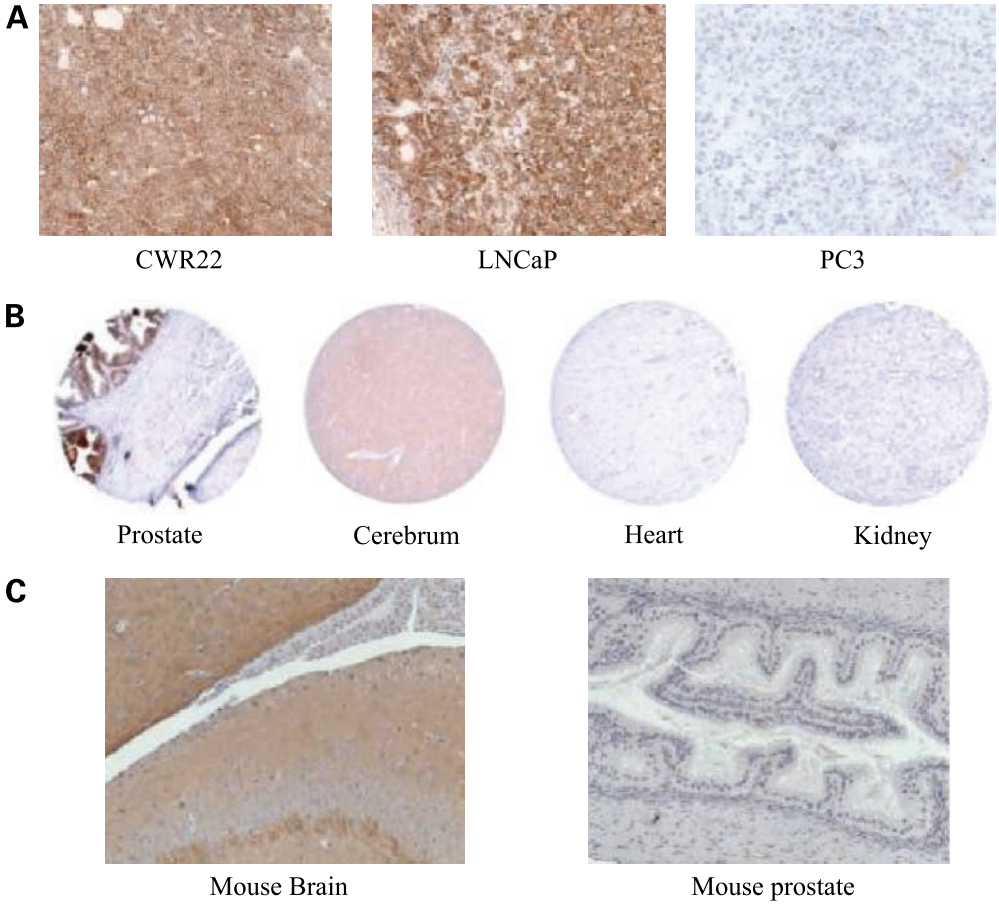

Figure 2. IHC analysis of human and mouse tissues. Pr1#19 mAb was used to stain formalin-fixed paraffin-embedded tissues. **A,** validation of Pr1#19 as an IHC reagent on the human prostate cancer xenografts CWR22, LNCaP, and PC3. **B,** staining of normal human tissues. **C,** staining of normal mouse tissues.

supernatants were selected based on off rates (K_D) for binding to covalently immobilized TMEFF2 extracellular domain as measured by BIAcore. Five hybridomas producing supernatants with the lowest dissociation rate constants were chosen for subcloning and purification. Purified mAbs were further evaluated by epitope mapping and affinity measurements by BIAcore. One mAb in particular, Pr1#19, recognized a unique epitope on human TMEFF2 with high affinity ($K_D = 2.32 \pm 0.45$ nmol/L). The mature murine TMEFF2 protein (National Center for Biotechnology Information reference sequence NP_062764.1; ref. 20) exhibits only two amino acid differences in the extracellular coding sequence relative to its human orthologue. BIAcore analysis showed that the epitope recognized by Pr1#19 is conserved between human and mouse and that the affinity for the mouse protein is similar to that of human ($K_D = 3.36 \pm 0.28$ nmol/L).

Table 1. IHC staining of normal human tissues with anti-TMEFF2 mAb Pr1#19

Tissue	Positive samples
Prostate	15/24
Cerebrum	8/12
Cerebellum	10/10

NOTE: Negative tissue samples are adrenal gland, bladder, blood, bone marrow, breast, colon, duodenum, endothelium, eye, fallopian tubes, heart, kidney, liver, lung, lymph node, ovary, pancreas, parathyroid, pituitary, skeletal muscle, skin, spinal cord, spleen, testes, thymus, thyroid, ureter, uterus, cervix, gallbladder, myometrium, peripheral nerve, salivary gland, stomach, and tonsil.

Pr1#19 was used in IHC analysis of normal and malignant human tissues to verify TMEFF2 protein expression. This mAb was validated as an IHC reagent by demonstrating that it recognized TMEFF2 protein in LNCaP and CWR22 xenograft sections, which are positive for TMEFF2 mRNA expression, but not in PC3 xenograft sections, which are negative for TMEFF2 mRNA expression (Figs. 1B and 2A). The staining was uniform in 100% of LNCaP and CWR22 cells and was cytoplasmic and membranous in nature.

IHC analysis of normal body tissues confirmed the gene chip data that only human central nervous system tissues and normal prostate express TMEFF2 protein (Fig. 2B and Table 1). The staining pattern in central nervous system tissues was largely diffuse staining of neural fibrils, white matter, and Purkinje cells. Normal prostate staining (15 of 24) was more distinct and restricted to the glandular epithelium. Prostate stroma, smooth muscle cells, and

basal cells were negative. The remainder of the 35 normal body tissues tested did not show detectable staining with Pr1#19 (Table 1). Analysis of normal mouse tissues showed TMEFF2 expression only in brain (5 of 5) but not in mouse prostate (0 of 2; Fig. 2C).

Analysis of primary prostate cancer specimens showed that TMEFF2-specific staining was restricted to the cytoplasm and membranes of the cancer epithelium (Fig. 3A). The prostate cancer cohort (n = 65) displayed weak (+1) to strong (+3) staining in 48 cases, demonstrating that a large fraction of prostate cancer patients exhibit expression of TMEFF2. More specifically, 112 of 222 separate prostate cancer elements stained positively for TMEFF2 expression. No significant correlation of anti-TMEFF2 staining with Gleason grade or stage of disease was observed (see summary in Table 2). Moderate staining was also seen in 5 of 6 cases of prostatic intraepithelial neoplasia and 15 of 17 cases of benign glands or hyperplasia adjacent to cancer (Fig. 3B and Table 2). TMEFF2 expression was also detected in four of six cases of locally advanced disease (D2 stage), indicating that expression of this target is retained in advanced disease (Fig. 3C).

To further examine advanced stage disease, 61 specimens derived primarily from lymph node and bone metastasis, including hormone-dependent and hormone-independent samples, were subjected to IHC analysis, and 25 samples were positive (summarized in Table 2 and examples in Fig. 3D and E). TMEFF2 protein expression was detected in 25% of hormone-dependent metastases, all positives being derived from lymph node lesions. Positive IHC staining was also observed in 48% of hormone-independent prostate cancers, wherein all but one specimen were derived from bone metastases. In addition, 6 of 10 metastases with unknown hormonal status expressed significant levels of TMEFF2. These results show that TMEFF2 expression persists through advanced stages of prostate cancer, including bone metastasis and hormone independence.

Table 2. IHC staining of prostate tissues with anti-TMEFF2 mAb Pr1#19

Pathology	Positive samples*
Hyperplasia	15/17
High-grade prostatic intraepithelial neoplasia	5/6
Cancer grade	
2	5/6
3	53/104
4	44/92
5	10/20
D2 stage	4/6
Lymph node metastases	
Hormone dependent	6/19
Hormone independent	1/6
Unknown status†	3/5
Bone metastases	
Hormone dependent	0/4
Hormone independent	12/18
Other metastases	
Hormone dependent‡	0/1
Hormone independent§	0/3
Unknown status‖	3/5

*Samples were classified as positive if ≥10% of invasive epithelial cells showed 1+ intensity staining or ≥1% of invasive (hyperplasia & high-grade prostatic intraepithelial neoplasia not invasive) epithelial cells showed 2+ to 3+ intensity staining.
†Lymph node metastases with unknown hormone status collected at the Garvan Institute of Medical Research.
‡ Liver metastasis.
§Two lung metastases and one paravertebral mass.
‖Unknown hormonal status and unknown metastatic site.

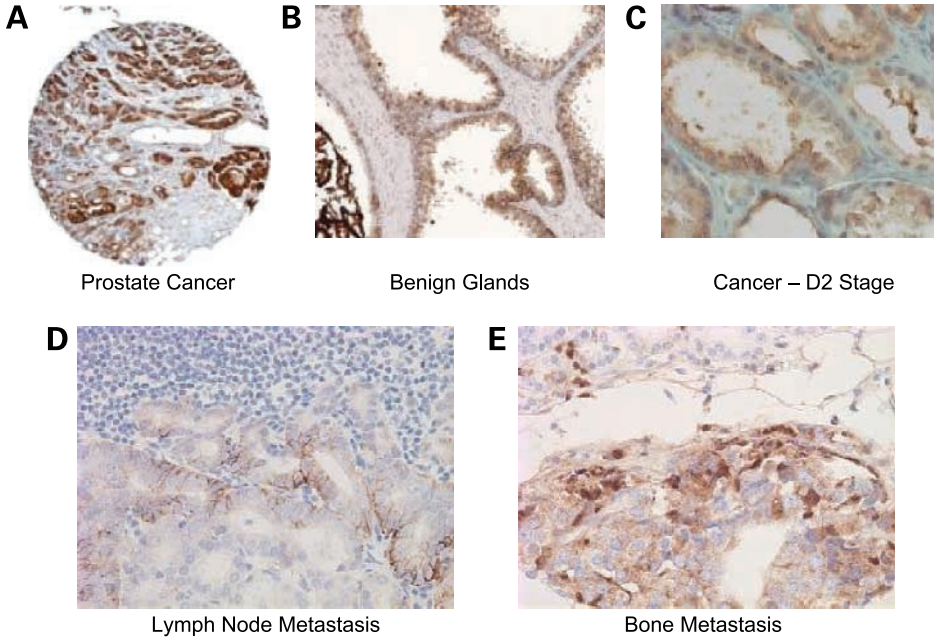

Figure 3. IHC analysis of human prostate cancer tissues. Pr1#19 mAb was used to stain formalin-fixed paraffin-embedded tissues. **A,** primary prostate tumor. **B,** benign gland adjacent to prostate cancer. **C,** D2 stage disease. **D,** lymph node metastasis of prostate cancer. **E,** bone metastasis of prostate cancer.

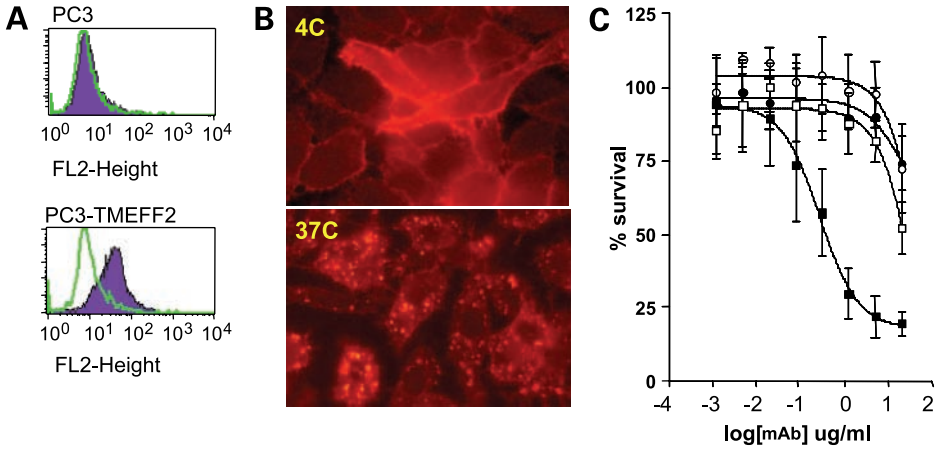

Figure 4. *In vitro* assays using anti-TMEFF2 antibody. **A,** flow cytometry analysis using Pr1#19 mAb shows cell surface protein expression in TMEFF2-transfected PC3 cells but not in parental PC3 cells. **B,** anti-TMEFF2 mAb Pr1#19 is rapidly internalized at 37°C in PC3-TMEFF2 cells. **C,** treatment of parental PC3 and TMEFF2-transfected PC3 cells with either Pr1-vcMMAE or a control ADC, TIB-vcMMAE. Cells were treated with ADC for 1 hour and assayed for cell survival at day 4 post-treatment. Treatment groups are parental PC3 treated with TIB-vcMMAE (*open circles*) or Pr1-vcMMAE (*solid circles*) and PC3-TMEFF2 treated with TIB-vcMMAE (*open squares*) or Pr1-vcMMAE (*solid squares*).

In vitro Killing by Toxin-Conjugated Anti-TMEFF2 mAb

Gene array and IHC data show that LNCaP but not PC3 prostate cancer cells express TMEFF2 (Figs. 1B and 2A). Flow cytometry analysis using Pr1#19 mAb showed that TMEFF2 protein is expressed at the cell surface of LNCaP (data not shown) and TMEFF2-transfected PC3 cells but not in parental PC3 cells (Fig. 4A). Interestingly, at 37°C, Pr1#19 is very rapidly (within 15–30 minutes) internalized into an endosomal compartment in PC3-TMEFF2 cells (Fig. 4B). This property of TMEFF2 was not anticipated from the original identification by expression profiling and bioinformatics analysis. However, the rapid internalization makes this particular antibody-antigen combination highly attractive for an ADC approach, because activation of certain peptide-linked ADCs is dependent on cathepsin B cleavage following internalization into lysosomes (8–10).

To test the idea that Pr1#19 can therapeutically target TMEFF2-expressing cells, Pr1#19 was conjugated to the microtubule toxin auristatin E through a cathepsin B–cleavable linker (9) designed to limit toxicity to cells that internalize the target-ADC complex to lysosomes. This ADC, termed Pr1-vcMMAE, was cytotoxic to PC3-TMEFF2 cells *in vitro* at an IC_{50} of 0.25 μg/mL, when cells were incubated with the ADC for 1 hour (Fig. 4C). Parental PC3 cells were insensitive to Pr1-vcMMAE. A control ADC, TIB-vcMMAE, was noncytotoxic to both PC3 and PC3-TMEFF2 cells at ≤1 μg/mL. Anti-TMEFF2 mAb internalization and Pr1-vcMMAE-mediated cell killing were also observed in LNCaP cells in culture (data not shown).

Pr1-vcMMAE Inhibits Tumor Growth *In vivo*

To examine the effects of Pr1-vcMMAE *in vivo*, LNCaP xenografts were grown in immune compromised male severe combined immunodeficient mice and allowed to reach 30 to 150 mm^3 (64 mm^3 average). Mice were randomized into groups and treated with Pr1-vcMMAE or a control vcMMAE-conjugated antibody. As shown in Fig. 5A, Pr1-vcMMAE (0.215 mg/kg auristatin E, i.e., ~5 mg/kg of ADC) delivered either i.p. or i.v. to LNCaP-bearing mice resulted in significant inhibition of tumor growth ($P < 0.000003$ for i.v. and $P < 0.005$ for i.p.). The growth inhibitory effect of Pr1-vcMMAE correlated well with a decrease in serum prostate-specific antigen levels, a serum protein often used as a marker for prostate tumor burden (33). Pr1-vcMMAE-treated mice exhibited serum prostate-specific antigen levels of <10 ng/mL at the end of the study, whereas control vcMMAE-treated mice had prostate-specific antigen levels of >100 ng/mL.

The Pr1-vcMMAE was well tolerated as assessed by body weight (Fig. 5B). In contrast, both groups of animals receiving the control ADC in which LNCaP tumors continued to grow had to be removed from the study at day 50 postimplantation due to weight loss exceeding 20% (as per Institutional Animal Care and Use Committee regulations). We have found that mice bearing LNCaP tumors are particularly susceptible to weight loss and that tumor-burdened mice often have to be sacrificed while the tumors are still relatively small (400–700 mm^3). Mice treated with Pr1-vcMMAE at first exhibited a slight decrease in weight, which was attributed to tumor burden. However, after several doses of Pr1-vcMMAE, weight stabilized and actually increased, indicating that Pr1-vcMMAE is well tolerated and protective against weight loss due presumably to its effect on tumor burden. This is of particular significance, given the full binding potential of Pr1#19 mAb to the mouse target.

Inhibition of Tumor Growth with a Humanized Pr1-vcMMAE

Murine antibodies elicit a strong immune response in the clinic in the form of human antimouse antibody response, risking inactivation of the therapeutic antibody. To eliminate this possibility and create a therapeutic more suitable for clinical trials, the murine Pr1#19 mAb was humanized (26). BIAcore analysis of the humanized Pr1#19 showed that it recognized human TMEFF2 protein with similar affinity ($K_D = 5.8 \pm 2.5$ nmol/L) compared with the murine Pr1#19 mAb. This humanized antibody (see Fig. 6A and B for sequence) was conjugated to auristatin E to create human Pr1-vcMMAE (huPr1-vcMMAE), the humanized version of the anti-TMEFF2 ADC. Initial studies

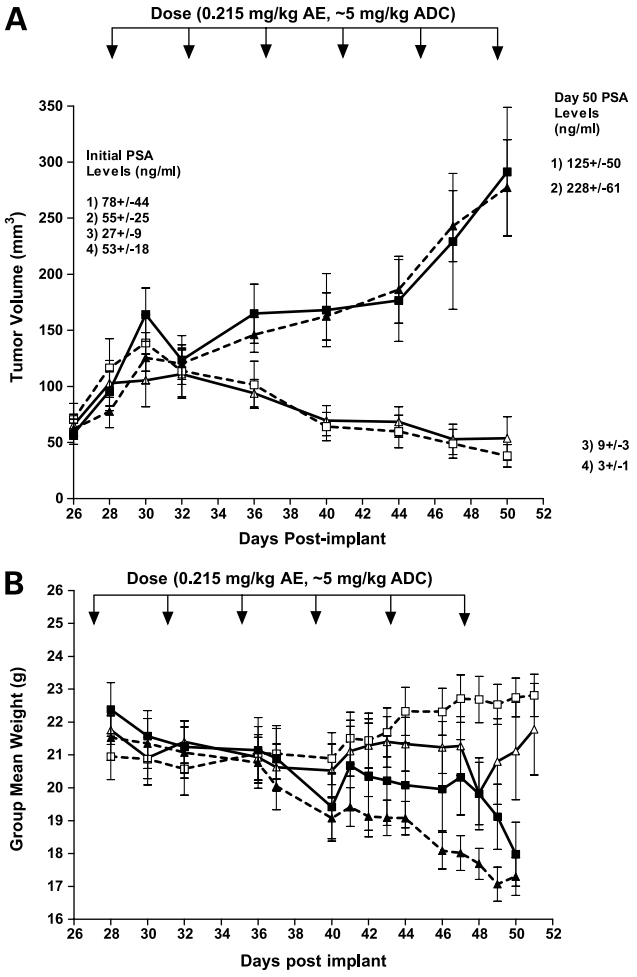

Figure 5. *In vivo* LNCaP tumor inhibition with Pr1-vcMMAE. **A,** Pr1-vcMMAE was given at 5 mg/kg i.v. or i.p. every 4 days to male severe combined immunodeficient mice bearing established LNCaP tumors. In comparison with control TIB-vcMMAE, Pr1-vcMMAE effectively inhibited LNCaP tumor growth. This inhibition was paralleled by a significant reduction in serum prostate-specific antigen. Multiple experiments with *in vivo* efficacy were done at ADC dose ranges of 3–10 mg/kg. **B,** mice treated with Pr1-vcMMAE did not have significant changes in body mass, indicating that this ADC was well tolerated. No obvious toxic effects were observed. Mice with a >20% decline in body weight, as was seen with tumor-bearing mice treated with vehicle or control ADC, were euthanized according to Institutional Animal Care and Use Committee protocols. Treatments are group 1, i.v. TIB-vcMMAE (*solid squares*); group 2, i.p. TIB-vcMMAE (*solid triangles*); group 3, i.v. Pr1-vcMMAE (*open squares*); and group 4, i.p. Pr1-vcMMAE (*open triangles*).

with LNCaP tumors grown *in vivo* showed that huPr1-vcMMAE had similar efficacy in growth inhibition compared with its murine counterpart (data not shown). To extend these studies and show that efficacy is not limited to a single *in vivo* model, we used the CWR22 xenograft model. Like LNCaP, and in contrast to the other prostate cancer lines PC3, DU145, and RPWE-2 cells, CWR22 expresses high levels of TMEFF2 mRNA and protein (Figs. 1B and 2A). Male severe combined immunodeficient mice were implanted with tumor chunks (1–3 mm^3) that were allowed to grow to an average of 115 mm^3 (range 35–215 mm^3). They were randomized into two groups and treated with huPr1-vcMMAE or control ADC. As seen in Fig. 6C, multiple doses of 0.215 mg/kg auristatin E (~5 mg/kg ADC) significantly inhibited the growth of the aggressive CWR22 tumor line ($P < 0.0005$). Several animals treated with six doses of the control ADC had to be sacrificed at day 38 postimplantation due to tumor size exceeding Institutional Animal Care and Use Committee regulations (as indicated). However, all animals treated with huPr1-vcMMAE remained on study until day 72 and tolerated 13 doses of the huPr1-vcMMAE. This ADC had similar efficacy at doses ranging from 0.135 to 0.44 mg/kg auristatin E (~3–10 mg/kg ADC), with both the original murine and the humanized version of the antibody proving equally effective (data not shown). These results show that huPr1-vcMMAE safely and effectively inhibits the growth of two distinct and aggressive prostate cancer xenograft models.

Discussion

Our goal was to identify a prostate cancer-specific gene and develop an ADC that would specifically target the gene product for the treatment of prostate cancer. We selected as our target *TMEFF2*, a gene with no defined function but with very restricted normal tissue expression and aberrantly high overexpression in prostate cancer. In addition, *TMEFF2* seemed particularly suitable as a target for a therapeutic ADC due to its high rate of internalization after ligation with an antibody.

TMEFF2 has been implicated in cell signaling (21), neuronal cell survival (20), and tumor suppression (22, 34, 35). The *TMEFF2* gene is hypermethylated in some cancers (22, 34), and overexpression led to inhibition of cell proliferation (35). The proposed tumor suppressor function is not supported in prostate cancer wherein our data and others (23, 36) report high expression of the wild-type gene. Heterologous overexpression of TMEFF2 in PC3 cells also did not have a negative effect on cell proliferation in our *in vitro* assays. Instead, TMEFF2 is likely associated with cell proliferation and emergence of hormone independence of prostate cancer xenografts, as has been suggested previously (23, 36), a conclusion supported by our observation of TMEFF2 expression in bone and lymph node metastases, many of which exhibited a hormone-independent phenotype.

The restricted tissue expression of TMEFF2 makes this gene product an attractive candidate for targeted therapy. We developed a specific ADC, huPr1-vcMMAE, consisting of a humanized anti-TMEFF2 mAb linked to auristatin E via a cathepsin B–cleavable linker as described by Doronina et al. (9). This ADC strongly inhibits the growth *in vitro* of PC3 cells overexpressing the antigen and of LNCaP and CWR22 prostate cancer xenografts *in vivo*. The efficacy in tumor growth inhibition was retained with humanization, which will reduce the risk of immune rejection of the ADC when tested in humans (26, 37).

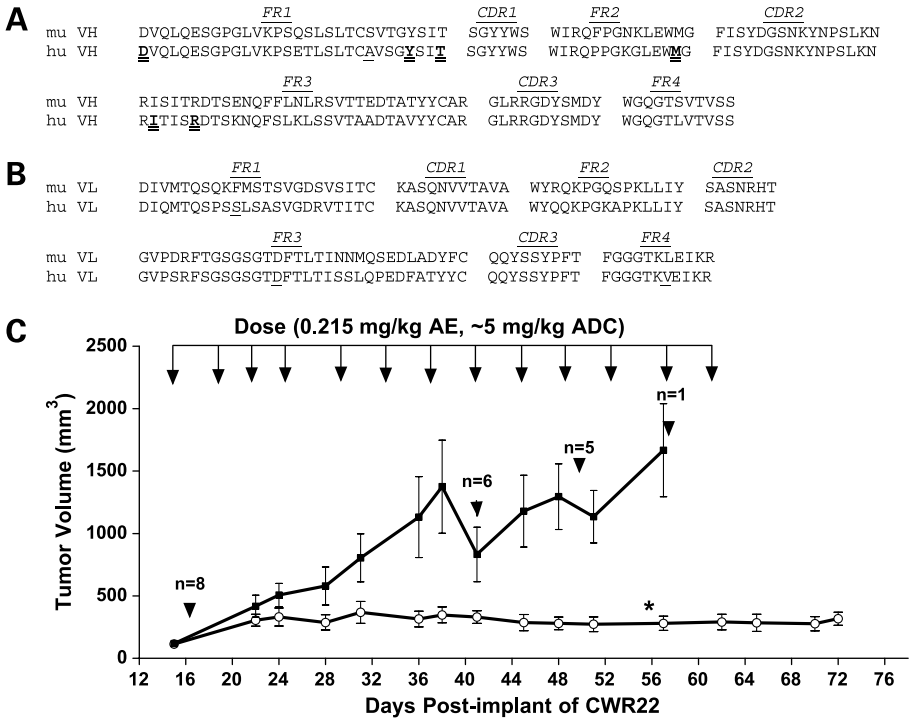

Figure 6. Humanized anti-TMEFF2 mAb and ADC. **A** and **B,** amino acid sequence alignment of mouse (*mu*) and humanized (*hu*) variable heavy (*VH*) and variable light (*VL*) domains and the complementarity determining regions (*CDR*) and framework regions (*FR*). *Bold with double underlining,* the six retained murine framework residues in the humanized variable heavy domain. *Single underlining,* framework residues changed to the more commonly found residues in human frameworks. **C,** *in vivo* tumor inhibition of CWR22 xenografts with huPr1-vcMMAE. ADC was given at 5 mg/kg i.p. every 4 days to male severe combined immunodeficient mice bearing established CWR22 tumors. In comparison with control TIB-vcMMAE (*solid squares*), huPr1-vcMMAE (*open circles*) effectively inhibited CWR22 tumor growth. At certain times, some animals in the control group had to be removed from study due to tumor size exceeding Institutional Animal Care and Use Committee regulations. *Arrows,* numbers of animals remaining on study. All eight animals in the huPr1-vcMMAE-treated group survived until the end of the study. *, $P < 0.0005$ (Student's *t* test).

Antigen density is often a factor in the therapeutic effectiveness of antibody-mediated therapies (8, 12, 38). Our data show that clinical prostate cancer samples express similar or greater levels of TMEFF2 when compared with either LNCaP or CWR22 cells (see Figs. 1 and 2). The strong efficacy of huPr1-vcMMAE is likely due to the efficient internalization of the ADC-antigen complex as seen with PC3-TMEFF2 cells *in vitro* (Fig. 4). The drug is presumably released via cathepsin B cleavage of the valine-citrulline linker (9) and likely exerts its cytotoxic effects via apoptosis (10).

Efficacy of huPr1-vcMMAE is observed at various doses ranging from 3 to 10 mg/kg. The free drug equivalents of these doses range from 0.14 to 0.44 mg/kg. This suggests that, even if the ADC were to completely disintegrate, the released auristatin E would be below the published maximum tolerated dose of free auristatin E (0.72 mg/kg; ref. 10).

The cathepsin B–cleavable valine-citrulline linker employed in the huPr1-vcMMAE ADC is extremely stable in human and mouse plasma (8–10) and is likely superior to either hydrazone and/or disulfide linkers employed in other ADCs (11, 12, 14, 39). Free drug release from an anti-CD30 vcMMAE ADC was only 2% to 5% after 10 days of incubation at 37°C (10). Similarly, an ADC toward Lewis Y antigen exhibited <5% free drug release in human plasma when conjugated via a valine-citrulline linker compared with >30% free drug release from a hydrazone linkage (9). Our data to date indicate no discernible nonspecific toxicity due to disintegration of the ADC in huPr1-vcMMAE-treated mice.

The maximum tolerated dose of huPr1-vcMMAE is unknown, as the highest dosing regimen tested to date (10 mg/kg for 12 doses) induced no detectable toxic side effects in mice. However, studies with other auristatin E conjugates using the same linker chemistry report a maximum tolerated dose of 30 to 40 mg/kg (9, 10). Other studies using ADCs for the treatment of prostate cancer have targeted prostate-specific membrane antigen (14) and prostate-specific cell antigen (12). Currently, anti–prostate-specific membrane antigen–specific ADCs using the disulfide-linked maytansinoid toxin DM1 are in phase I clinical trials (14). Whereas no preclinical tumor studies have been published with DM1-conjugated anti–prostate-specific membrane antigen ADCs, a recent study shows anti-LNCaP tumor efficacy in nude mice with a radiolabeled anti–prostate-specific membrane antigen mAb (40). Aside from targeting a different antigen, huPr1-vcMMAE differs from the anti–prostate-specific cell antigen and anti–prostate-specific membrane antigen ADCs in two important aspects. As described above, huPr1-vcMMAE exhibits the more stable valine-citrulline linker, suggesting a longer half-life and a greater safety profile of the ADC. Secondly, the mAb used to target TMEFF2 very effectively cross-reacts with murine TMEFF2. The significance of this is that the xenograft mouse models used to test huPr1-vcMMAE allowed evaluation of both efficacy and toxicity of the ADC. IHC analysis of mouse tissues with Pr1#19 showed expression in mouse brain, similar to that observed in human tissues (see also ref. 41). Other mouse tissues, including mouse prostate, did not express TMEFF2 protein. The basis of expression in normal human prostate and

not normal mouse prostate remains to be determined. Despite expression in the mouse brain, no overt neurotoxicity and/or pathology was observed in mice treated with huPr1-vcMMAE even at multiple doses of 10 mg/kg. In fact, mice bearing LNCaP tumors treated with Pr1-vcMMAE seemed healthier and did not experience tumor-associated weight loss when compared with tumor-bearing mice treated with a control ADC. This suggests that huPr1-vcMMAE does not cross the blood-brain barrier but effectively reaches the tumor cells and exerts a cytotoxic effect only to the TMEFF2-expressing tumors.

In summary, huPr1-vcMMAE specifically targets a gene product that is overexpressed at all stages of prostate cancer. Our *in vivo* studies suggest that this drug exhibits a large therapeutic window, demonstrating efficacy at the lowest dose tested (3 mg/kg) and showing no signs of toxicity at the highest dose tested (10 mg/kg). Given the efficacy of this experimental therapeutic in animal models of prostate cancer, we propose that huPr1-vcMMAE may be a reasonable experimental therapeutic for humans with metastatic and hormone-resistant prostate cancer, following completion of further and more extensive animal toxicity studies.

Acknowledgments

We thank Max Vasquez, Peter Senter, and Yuni Fang for critical reading of this manuscript and Jennifer Miller for excellent technical assistance.

References

1. Smaletz O, Scher HI. Outcome predictions for patients with metastatic prostate cancer. Semin Urol Oncol 2002;20:155 – 63.

2. Beer TM, Garzotto M, Henner WD, Eilers KM, Wersinger EM. Intermittent chemotherapy in metastatic androgen-independent prostate cancer. Br J Cancer 2003;89:968 – 70.

3. Meluch AA, Greco FA, Morrissey LH, et al. Weekly paclitaxel, estramustine phosphate, and oral etoposide in the treatment of hormone-refractory prostate carcinoma: results of a Minnie Pearl Cancer Research Network phase II trial. Cancer 2003;98:2192 – 8.

4. Petrylak DP. Chemotherapy for androgen-independent prostate cancer. Semin Urol Oncol 2002;20:31 – 5.

5. Autorino R, Di Lorenzo G, Damiano R, De Placido S, D'Armiento M. Role of chemotherapy in hormone-refractory prostate cancer. Old issues, recent advances and new perspectives. Urol Int 2003;70:1 – 14.

6. Braslawsky GR, Edson MA, Pearce W, Kaneko T, Greenfield RS. Antitumor activity of Adriamycin (hydrazone-linked) immunoconjugates compared with free Adriamycin and specificity of tumor cell killing. Cancer Res 1990;50:6608 – 14.

7. Bernstein ID. Monoclonal antibodies to the myeloid stem cells: therapeutic implications of CMA-676, a humanized anti-CD33 antibody calicheamicin conjugate. Leukemia 2000;14:474 – 5.

8. Bhaskar V, Law DA, Ibsen E, et al. E-selectin up-regulation allows for targeted drug delivery in prostate cancer. Cancer Res 2003;63: 6387 – 94.

9. Doronina SO, Toki BE, Torgov MY, et al. Development of potent monoclonal antibody auristatin conjugates for cancer therapy. Nat Biotechnol 2003;21:778 – 84.

10. Francisco JA, Cerveny CG, Meyer DL, et al. cAC10-vcMMAE, an anti-CD30-monomethyl auristatin E conjugate with potent and selective antitumor activity. Blood 2003;102:1458 – 65.

11. Liu C, Tadayoni BM, Bourret LA, et al. Eradication of large colon tumor xenografts by targeted delivery of maytansinoids. Proc Natl Acad Sci USA 1996;93:8618 – 23.

12. Ross S, Spencer SD, Holcomb I, et al. Prostate stem cell antigen as therapy target: tissue expression and *in vivo* efficacy of an immunoconjugate. Cancer Res 2002;62:2546 – 53.

13. Tolcher AW, Ochoa L, Hammond LA, et al. Cantuzumab mertansine, a maytansinoid immunoconjugate directed to the CanAg antigen: a phase I, pharmacokinetic, and biologic correlative study. J Clin Oncol 2003;21:211 – 22.

14. Bander NH, Nanus DM, Milowsky MI, Kostakoglu L, Vallabahajosula S, Goldsmith SJ. Targeted systemic therapy of prostate cancer with a monoclonal antibody to prostate-specific membrane antigen. Semin Oncol 2003;30:667 – 76.

15. Bubendorf L, Kolmer M, Kononen J, et al. Hormone therapy failure in human prostate cancer: analysis by complementary DNA and tissue microarrays. J Natl Cancer Inst 1999;91:1758 – 64.

16. Luo J, Duggan DJ, Chen Y, et al. Human prostate cancer and benign prostatic hyperplasia: molecular dissection by gene expression profiling. Cancer Res 2001;61:4683 – 8.

17. Welsh JB, Sapinoso LM, Su AI, et al. Analysis of gene expression identifies candidate markers and pharmacological targets in prostate cancer. Cancer Res 2001;61:5974 – 8.

18. Luo J, Isaacs WB, Trent JM, Duggan DJ. Looking beyond morphology: cancer gene expression profiling using DNA microarrays. Cancer Invest 2003;21:937 – 49.

19. Henshall SM, Afar DE, Rasiah KK, et al. Expression of the zinc transporter ZnT4 is decreased in the progression from early prostate disease to invasive prostate cancer. Oncogene 2003;22:6005 – 12.

20. Horie M, Mitsumoto Y, Kyushiki H, et al. Identification and characterization of TMEFF2, a novel survival factor for hippocampal and mesencephalic neurons. Genomics 2000;67:146 – 52.

21. Uchida T, Wada K, Akamatsu T, et al. A novel epidermal growth factor-like molecule containing two follistatin modules stimulates tyrosine phosphorylation of erbB-4 in MKN28 gastric cancer cells. Biochem Biophys Res Commun 1999;266:593 – 602.

22. Liang G, Robertson KD, Talmadge C, Sumegi J, Jones PA. The gene for a novel transmembrane protein containing epidermal growth factor and follistatin domains is frequently hypermethylated in human tumor cells. Cancer Res 2000;60:4907 – 12.

23. Glynne-Jones E, Harper ME, Seery LT, et al. TENB2, a proteoglycan identified in prostate cancer that is associated with disease progression and androgen independence. Int J Cancer 2001;94:178 – 84.

24. Henshall SM, Afar DE, Hiller J, et al. Survival analysis of genome-wide gene expression profiles of prostate cancers identifies new prognostic targets of disease relapse. Cancer Res 2003;63:4196 – 203.

25. Kabat EA, Wu TT, Perry HM, Gottesman KS, Foeller C. Sequences of proteins of immunological interest. 5th ed. Washington (DC): U.S. Department of Health and Human Services, NIH; 1991.

26. Queen C, Schneider WP, Selick HE, et al. A humanized antibody that binds to the interleukin 2 receptor. Proc Natl Acad Sci USA 1989;86: 10029 – 33.

27. Wang X, Stollar BD. Immunoglobulin VH gene expression in human aging. Clin Immunol 1999;93:132 – 42.

28. van Den Brink EN, Turenhout EA, Davies J, et al. Human antibodies with specificity for the C2 domain of factor VIII are derived from VH1 germline genes. Blood 2000;95:558 – 63.

29. Stemmer WP, Crameri A, Ha KD, Brennan TM, Heyneker HL. Single-step assembly of a gene and entire plasmid from large numbers of oligodeoxyribonucleotides. Gene 1995;164:49 – 53.

30. Kononen J, Bubendorf L, Kallioniemi A, et al. Tissue microarrays for high-throughput molecular profiling of tumor specimens. Nat Med 1998; 4:844 – 7.

31. Horoszewicz JS, Leong SS, Kawinski E, et al. LNCaP model of human prostatic carcinoma. Cancer Res 1983;43:1809 – 18.

32. Pretlow TG, Wolman SR, Micale MA, et al. Xenografts of primary human prostatic carcinoma. J Natl Cancer Inst 1993;85:394 – 8.

33. Dixon SC, Knopf KB, Figg WD. The control of prostate-specific antigen expression and gene regulation by pharmacological agents. Pharmacol Rev 2001;53:73 – 91.

34. Young J, Biden KG, Simms LA, et al. HPP1: a transmembrane protein-encoding gene commonly methylated in colorectal polyps and cancers. Proc Natl Acad Sci USA 2001;98:265 – 70.

35. Gery S, Sawyers CL, Agus DB, Said JW, Koeffler HP. TMEFF2 is an androgen-regulated gene exhibiting antiproliferative effects in prostate cancer cells. Oncogene 2002;21:4739 – 46.

36. Mohler JL, Morris TL, Ford OH III, Alvey RF, Sakamoto C, Gregory CW. Identification of differentially expressed genes associated with androgen-independent growth of prostate cancer. Prostate 2002;51: 247 – 55.

37. Co MS, Queen C. Humanized antibodies for therapy. Nature 1991; 351:501 – 2.

38. Hooijberg E, Sein JJ, van den Berk PC, et al. Eradication of large human B cell tumors in nude mice with unconjugated CD20 monoclonal antibodies and interleukin 2. Cancer Res 1995;55:2627 – 34.

39. Trail PA, Willner D, Knipe J, et al. Effect of linker variation on the stability, potency, and efficacy of carcinoma-reactive BR64-doxorubicin immunoconjugates. Cancer Res 1997;57:100 – 5.

40. Vallabhajosula S, Smith-Jones PM, Navarro V, Goldsmith SJ, Bander NH. Radioimmunotherapy of prostate cancer in human xenografts using monoclonal antibodies specific to prostate specific membrane antigen (PSMA): studies in nude mice. Prostate 2004;58:145 – 55.

41. Kanemoto N, Horie M, Omori K, et al. Expression of TMEFF1 mRNA in the mouse central nervous system: precise examination and comparative studies of TMEFF1 and TMEFF2. Brain Res Mol Brain Res 2001;86: 48 – 55.